Turkish Journal of Electrical Engineering & Computer Sciences

http://journals.tubitak.gov.tr/elektrik/

Research Article

Turk J Elec Eng & Comp Sci
(2017) 25: 3839 – 3853

doi:10.3906/elk-1606-435

Robust control for line-of-sight stabilization of a two-axis gimbal system

Mehmet BASKIN[1,*], **Kemal LEBLEBİCİOĞLU**[2]

[1]Control Systems Design, MGEO, Aselsan Inc., Ankara, Turkey

[2]Department of Electrical & Electronics Engineering, Faculty of Engineering, Middle East Technical University, Ankara, Turkey

Received: 26.06.2016 • **Accepted/Published Online:** 16.06.2017 • **Final Version:** 05.10.2017

Abstract: Line-of-sight stabilization against various disturbances is an essential property of gimbaled imaging systems mounted on mobile platforms. In recent years, the importance of target detection from higher distances has increased. This has raised the need for better stabilization performance. For that reason, stabilization loops are designed such that they have higher gains and larger bandwidths. As these are required for good disturbance attenuation, sufficient loop stability is also needed. However, model uncertainties around structural resonances impose strict restrictions on sufficient loop stability. Therefore, to satisfy high stabilization performance in the presence of model uncertainties, robust control methods are required. In this paper, a robust controller design in LQG/LTR, H_∞, and μ-synthesis framework is described for a two-axis gimbal. First, the performance criteria and weights are determined to minimize the stabilization error with moderate control effort under known platform disturbance profile. Second, model uncertainties are determined by considering locally linearized models at different operating points. Next, robust LQG/LTR, H_∞, and μ controllers are designed. Robust stability and performance of the three designs are investigated and compared. The paper finishes with the experimental performances to validate the designed robust controllers.

Key words: LQG/LTR, H_∞, μ-synthesis, two-axis gimbal, robust multivariable control

1. Introduction

For precise pointing and tracking performance, line-of-sight (LOS) stabilization against various disturbances is essential for imaging systems. To obtain better performance, bandwidth and gain of stabilization loops need to be increased while sufficient loop stability is maintained. For gimbaled imaging systems, the main difficulties in satisfying sufficient loop stability and good performance at the same time are model uncertainties around structural resonances. Therefore, robust control methods are needed to maintain high stabilization performance under model uncertainties. In this aspect, this paper deals with the design of a stabilization loop for a two-axis gimbal.

Classical control methods were used for stabilization loops in the past [1,2]. However, finding a classical controller that satisfies both stability and performance criteria is a time-consuming iterative procedure. Moreover, this method suffers from lack of optimality. Over the past decade, different methods have been used to obtain good stability and performance properties. Linear quadratic methods [3–5], H_∞ control methods [6-8], and μ-synthesis [9] are applied to the LOS control problem. However, in most of these reports the performance is evaluated only for nominal models. In other words, the stability and performance change due to model

*Correspondence: mbaskin@aselsan.com.tr

uncertainty are not considered. In addition, although some designers conduct an analysis for robustness, there are not clear experimental data to validate the robustness of the stabilization loops. Therefore, in this paper the authors try to fully support all theoretical findings with experimental data.

In the next section, three controller design methods are reviewed. Firstly, LQG/LTR design is discussed. In traditional LQG method, the desired loop shape is obtained by adjusting weighting matrices or intensities of process and measurement noises. However, in this paper a different approach is followed to shape the loop easily [10,11]. By using this modified technique, the sensitivity is successfully shaped for good disturbance rejection. Next, H_∞ and μ-synthesis design in mixed sensitivity framework are investigated. In previous mixed sensitivity designs, performance and uncertainty weights are determined by using general rules. However, in this paper all weights are determined by using experimental data. After designing three controllers, the performance and stability of the three designs are investigated and compared. Firstly, the comparison is made by investigating theoretical results. Next, experimental findings are obtained, and they are compared with theoretical results. Both theoretical and experimental results show that the stabilization loop has robust stability and robust performance properties for each of the three design methods.

2. Design methods

2.1. LQG/LTR design

The traditional LQG method uses a linear time invariant plant, and it assumes that the uncertainty in the states and measurements are additive [10]. The state space form of the plant is represented as in (1), where w_d and w_n are uncorrelated zero mean white noise processes having constant power spectral densities W and V as illustrated in (2).

$$\begin{aligned} \dot{x} &= Ax + Bu + \Gamma w_d \\ y &= Cx + w_n \end{aligned} \tag{1}$$

$$\begin{gathered} E\left\{w_d(t)\, w_d^T(\tau)\right\} = W\delta(t-\tau), \\ E\left\{w_n(t)\, w_n^T(\tau)\right\} = V\delta(t-\tau),\ E\left\{w_d(t)\, w_n^T(\tau)\right\} = 0 \end{gathered} \tag{2}$$

The aim of the LQG theory is to find a feedback control law to minimize the cost (3), where $Q = Q^T \geq 0$ and $R = R^T > 0$ are weighting matrices.

$$J = \lim_{T\to\infty} E\left\{\int_0^T \left(x^T Q x + u^T R u\right) dt\right\} \tag{3}$$

The solution turns out to be a cascade connection of Kalman filter and LQ regulator, each of which can tolerate gain variation between $(1/2,\ \infty)$ and phase variation less than 60° in each channel [10]. However, the cascaded form, LQG regulator, does not have guaranteed stability margins, and the closed loop may suffer from poor stability [11]. If one applies loop transfer recovery (LTR), the closed loop recovers the good stability properties of the Kalman filter [12]. Since the overall loop approaches the Kalman filter, good Kalman filter shape is essential for good disturbance rejection. In most of the reported designs, the desired Kalman filter shape is obtained by iteratively changing covariance matrices W and V. On the other hand, if frequency dependent weighting matrices $W(s)$ and $V(s)$ are used, to obtain a good Kalman filter is simpler [11,13]. As given in Figure 1, assume that instead of state disturbances the plant has output disturbance d and measurement noise v, which have power spectral density $D(s)$ and $V\ (s)$, respectively. An augmented system can be obtained

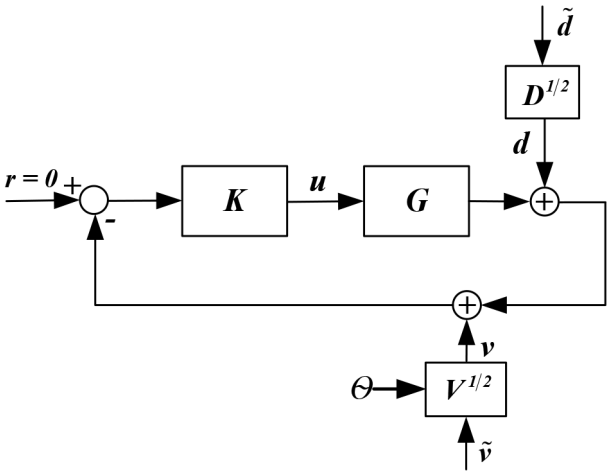

Figure 1. Plant augmentation.

if the states of the plant and frequency dependent weights are combined. If one assumes that $\tilde{d}$, $\tilde{v}$, and θ are uncorrelated white noises that satisfy (4), an LQG regulator for this augmented system can be designed [11,13].

$$E\left\{\theta(t)\,\theta^T(\tau)\right\} > 0,\ E\left\{\theta(t)\,\tilde{v}^T(\tau)\right\} = 0,\\ E\left\{\theta(t)\,\tilde{d}^T(\tau)\right\} = 0 \tag{4}$$

If the designer applies the LTR procedure for this augmented plant, the cost of the LTR procedure converges to (5) as the control weight approaches zero [11].

$$\lim_{R=\rho I,\ \rho\to 0} J_{LTR} = \frac{1}{2\pi}\int_{-\infty}^{\infty}\left\{\begin{array}{l}\sum\limits_i \sigma^2\left[S_o D^{1/2}(jw)\right]\\ +\sum\limits_i \sigma^2\left[T_o V^{1/2}(jw)\right]\end{array}\right\} dw \tag{5}$$

It can be seen that the LTR procedure applied at the plant output trades off the output sensitivity $S_o(jw)$ against the output complementary sensitivity $T_o\ (jw)$ with a factor $W_e\ (jw) = D^{1/2}(jw)\ V^{-1/2}(jw)$. It is a reasonable choice to take V as identity and $D^{1/2}$ as inverse of the desired sensitivity. If loop recovery is applied, the sensitivity can be shaped for good disturbance rejection. In the end, a closed loop having good stability and performance properties can be obtained.

2.2. H_∞ design

H_∞ design is made in a mixed sensitivity framework. In this method, sensitivity S_o is shaped for good disturbance rejection and KS_o is shaped to limit the control effort. Similarly, T_o is shaped for robust stability under multiplicative uncertainty. Therefore, cost (6) is used, and the corresponding linear fractional transformation (LFT) structure is given in Figure 2.

$$\left\| \begin{bmatrix} W_e S_o \\ W_u K S_o \\ W_t T_o \end{bmatrix} \right\|_\infty \tag{6}$$

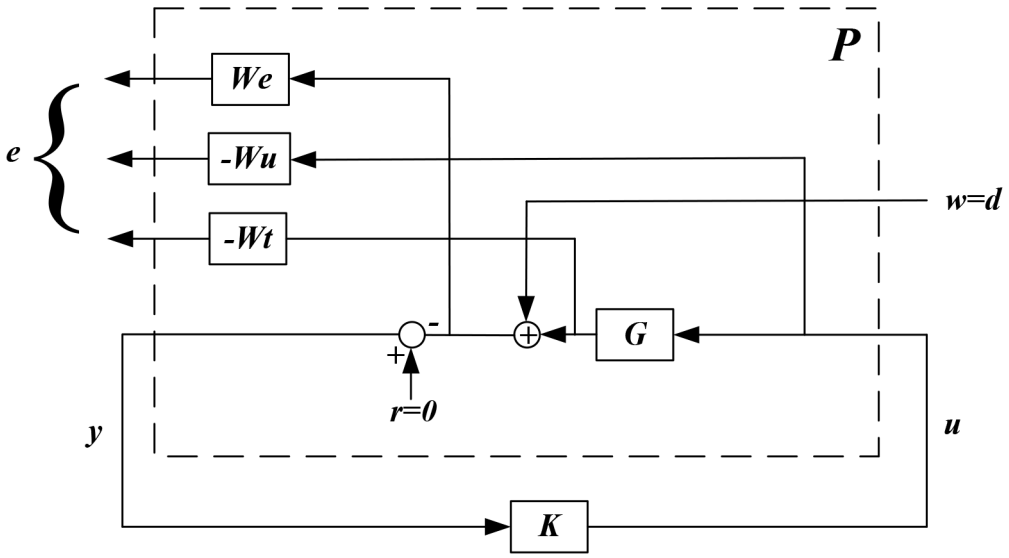

Figure 2. S/KS/T mixed sensitivity in regulation mode.

The aim of H_∞ control is to minimize cost (6) to satisfy the nominal performance and robust stability. In other words, it does not try to achieve robust performance unlike μ-synthesis. However, if the designer selects the weights carefully, the corresponding design may also satisfy the robust performance criterion similar to the μ-synthesis case.

2.3. μ-Synthesis design

$\mu-$Synthesis design is also made in a mixed sensitivity framework. For μ-synthesis design, robustness is gained by D-K iterations [14,15]. Therefore, cost only includes weighted S_o and KS_o as given by (7). Please observe that the aim of the μ-synthesis is to minimize (7) for all models in the complex set Δ to satisfy robust performance. For this design, the LFT structure in Figure 3 is used [13].

$$\left\| \begin{bmatrix} W_e S_o \\ W_u K S_o \end{bmatrix} \right\|_\infty \tag{7}$$

3. Two-axis gimbal model

The dynamic equations of the azimuth-elevation gimbal were derived in [16] previously. The equations illustrate that there are unwanted torque components if the gimbal is not dynamically mass balanced. However, in practical applications these gimbals are designed in such a way that they are approximately mass balanced. Under this assumption, these unwanted torque components become approximately zero for elevation axis. For the azimuth axis, they could not be eliminated totally, and some components that include high order angular velocity terms remain [16]. Since these angular velocities are usually small, (around 0.025 rad/s rms for this application) these components can be neglected. Therefore, the azimuth and elevation equations can be decoupled. In other words, the angular rate of any axis depends only on the net torque applied to that axis. For each axis, the resulting simplified model depicted in Figure 4 can be used for controller design. In this model, static friction can be viewed as an uncertainty source in low frequencies. Therefore, this model can be linearized around an operating point and it can be represented with a transfer function (8).

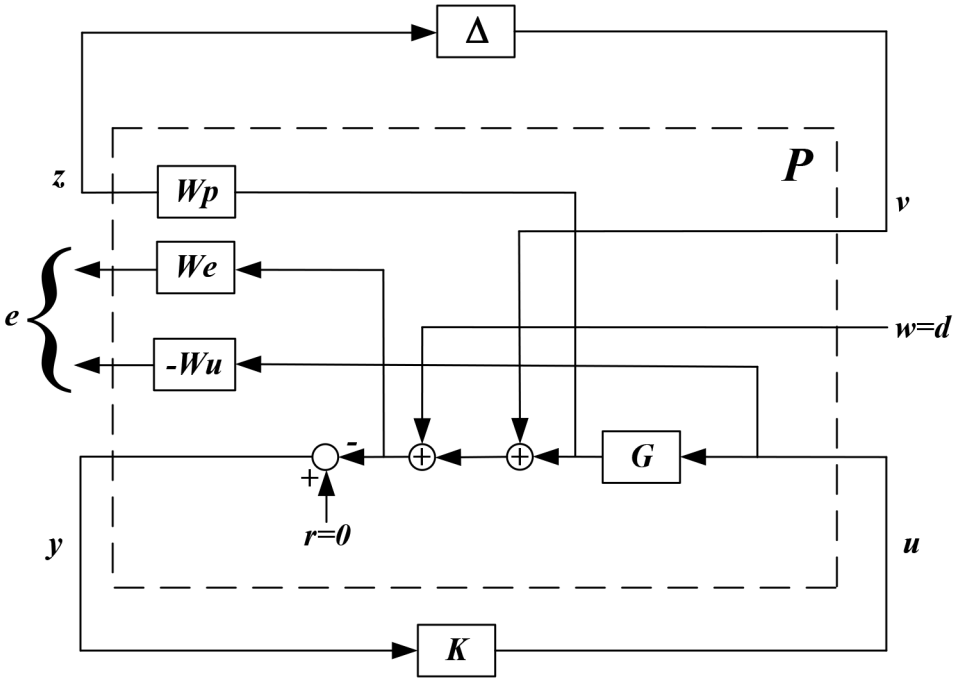

Figure 3. LFT structure for -synthesis.

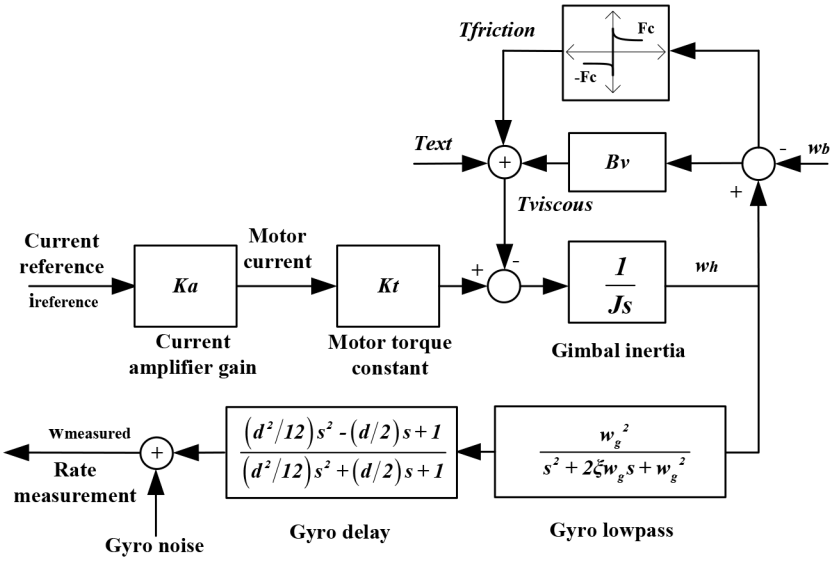

Figure 4. Gimbal model for one axis.

$$G(s) = \frac{w_{measured}}{i_{reference}} = \frac{K_a K_t}{Js + B_v} \times \frac{w_g^2}{s^2 + 2\xi w_g s + w_g^2} \times \frac{(d^2/12)\ s^2 - (d/2)\ s + 1}{(d^2/12)\ s^2 + (d/2)\ s + 1} \tag{8}$$

In model (8), pure time delay of the angular speed sensor (gyro) is approximated with a second order Pade function. This is an essential procedure to minimize the uncertainty at the mid-frequencies.

Some parameters of model (8) are easily obtainable from datasheets of the motor, driver, and gyro. However, determination of inertia J and viscous constant B_v requires more complicated analysis. For that

reason, extended Kalman filtering is used to identify the unknown parameters of the system [3,13]. These known and identified parameters are listed in Table 1. Moreover, the setup where all experimental tests are conducted is illustrated in Figure 5.

Table 1. Parameters of the system.

Parameters	Values
Current amplifier gain, K_a	2 A/A
Motor torque constant, K_t	2.18 Nm/A
Natural frequency of rate gyro, w_g	1646 rad/s
Damping of gyro, ξ	0.8
Gyro delay, d	4.5 ms
Azimuth inertia J	0.1736 kgm^2
Azimuth viscous constant B_v	1.15 Nm/(rad/s)
Elevation inertia J	0.063 kgm^2
Elevation viscous constant B_v	0.61 Nm/(rad/s)

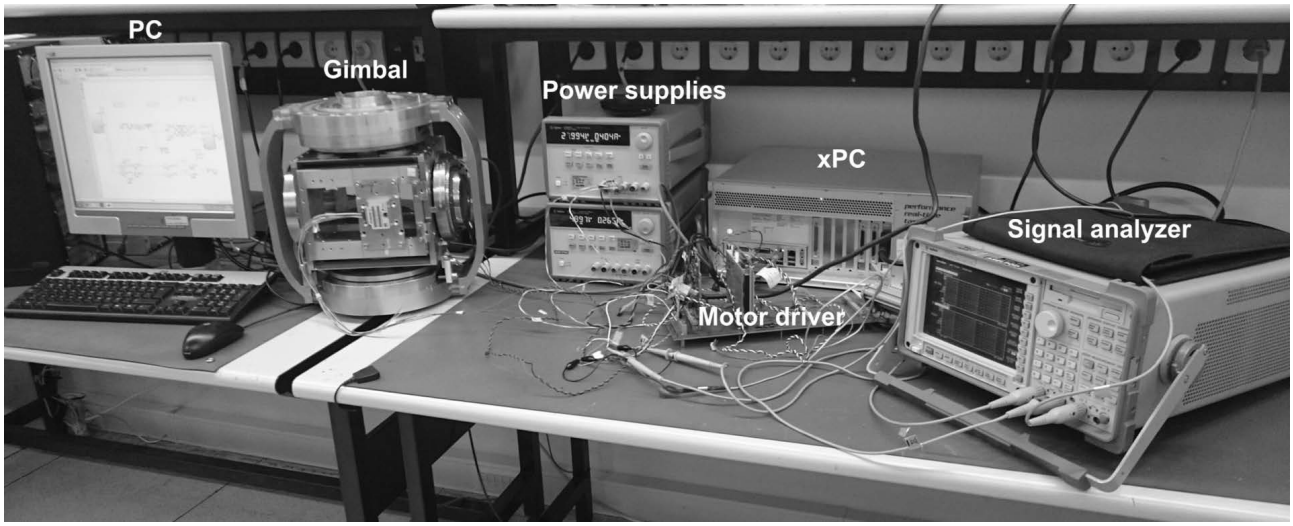

Figure 5. Experimental setup.

4. Nominal model construction

The linearized two-input two-output (TITO) gimbal model can be represented with (9), where w_{az}, w_{el}, i_{az}, and i_{el} are the azimuth and elevation angular rates and current inputs to the corresponding axes' motors.

$$\begin{bmatrix} w_{az} \\ w_{el} \end{bmatrix} = \begin{bmatrix} G_{11} & G_{12} \\ G_{21} & G_{22} \end{bmatrix} \begin{bmatrix} i_{az} \\ i_{el} \end{bmatrix} \tag{9}$$

In (9), G_{11} and G_{22} are the azimuth and elevation transfer functions obtained by evaluating (8) with the corresponding parameters listed in Table 1. Furthermore, G_{12} and G_{21} can be accepted as zero when the gimbal is mass balanced. This assumption is also applicable for the experimental setup displayed in Figure 5 [13]. In short, a nominal TITO model for the two-axis gimbal is constructed and this model will be used in the next sections.

5. Design descriptions

The main objective of LOS stabilization is to minimize pointing error due to platform motions. In electro-optical imaging systems, root mean square (rms) of LOS error must be smaller than a single detector pixel radiation angle for accurate target detection. In this project, the main motivation is to hold the rms LOS error under 75 microradians (μrad). Moreover, this aim must be achieved without saturating the motors and under model uncertainty. In this section, the weights that make this possible will be investigated.

5.1. Sensitivity and control weight selection

To determine the required loop shape and corresponding weights, the disturbance profile that the gimbal encounters is needed. In this application, this profile is obtained by measuring the three-axis angular speed of the platform in operational conditions. It is assumed that these angular speed disturbances act at the plant output.

The LOS error can be obtained by scaling platform angular position disturbances with the output sensitivity (S_o) of the rate loop. For that reason, position disturbances are obtained by integrating the angular speed data. The power spectrums of these position disturbances are displayed in Figure 6a. The spectrums show that the disturbances are dominant below 10 Hz. Eq. (10) suggests the relation between LOS error spectral density G_e and platform angular position spectral density G_p. If the pointing process is assumed to be zero mean, the rms error can be obtained by evaluating (11) at the required frequencies.

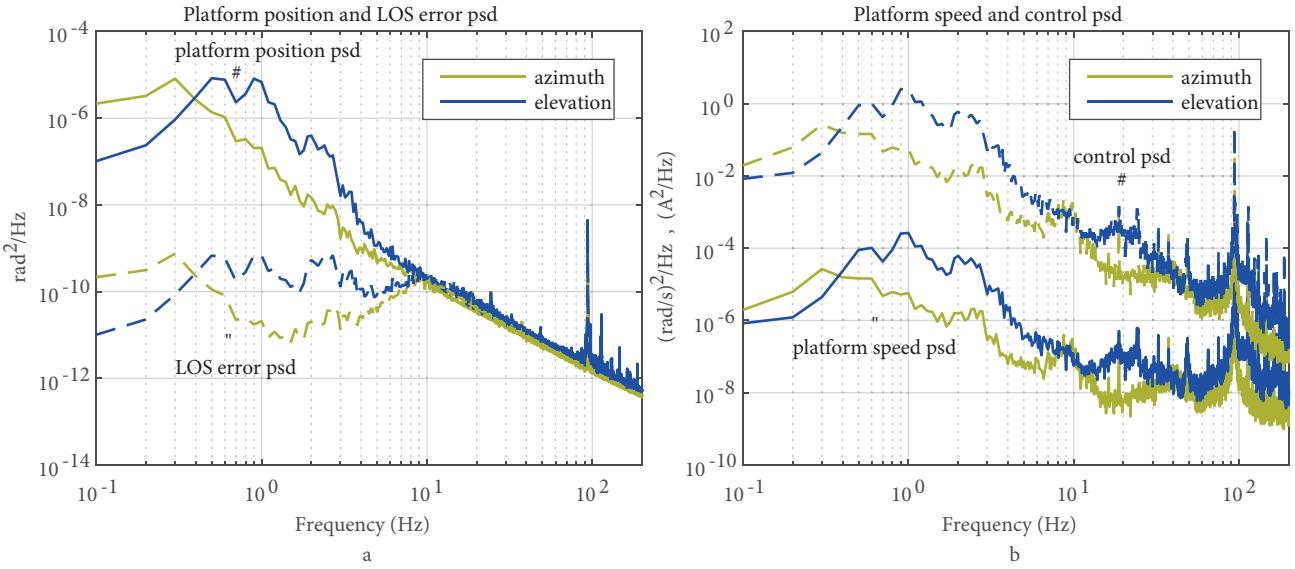

Figure 6. Power spectral density of (a) platform angular position (solid) and LOS error (dashed), (b) platform angular speed (solid) and control (dashed).

$$G_e(f) = |S_o(f)|^2 G_p(f) \tag{10}$$

$$e_{rms} = \sqrt{\int_{f1}^{f2} G_e(f)\, df} \tag{11}$$

Since the disturbances are small above 10 Hz, flat 5×10^{-10} rad^2/Hz error density in this region gives approximately 75 μrad rms error. According to (10), this is achieved by attenuating the disturbances more than 100 times below 1 Hz. Moreover, –40 db/decade slope is required to satisfy 10 Hz bandwidth. Therefore, the transfer function (12) is a good sensitivity selection. With this function, LOS error densities in Figure 6a are obtained. By evaluating (11) until 200 Hz, 52 and 74 μrad rms errors are obtained for the azimuth and elevation axes, respectively.

$$\begin{aligned} S_o &= \frac{s^2+2\xi w_b s\sqrt{\varepsilon}+w_b^2\varepsilon}{s^2/M_s+2\xi w_b s/\sqrt{M_s}+w_b^2}, \\ M_s &= 1,\ \varepsilon = 0.01,\ \xi = 0.5, w_b = 2\pi \times 10 \end{aligned} \tag{12}$$

Similarly, the control effort can be obtained by scaling platform angular speed disturbances with output sensitivity and controller (KS_o) of the rate loop. The power spectrums of these speed disturbances are displayed in Figure 6b. In this application, control effort smaller than 1.5 ampere (A) rms is desired for both axes. Similar to the sensitivity case, gain of KS_o function can be at most 100 in the desired bandwidth as displayed in Figure 6b. Beyond the loop bandwidth, gains must be reduced. Therefore, the transfer function (13) is a good KS_o selection. With this function, control densities in Figure 6b are obtained, and 0.4 and 1.35 A rms control efforts are obtained for the azimuth and elevation axes, respectively.

$$KS_o = \frac{\varepsilon_1 s + w_{bc}}{s + w_{bc}/M_u},\ M_u = 100, \varepsilon_1 = 0.01,\ w_{bc} = 2\pi \times 1200 \tag{13}$$

In this way, two desired closed loop transfer functions are obtained. Therefore, the sensitivity and control weights (14) and (15) can be used for each channel. Similarly, the weights (16) are used for TITO model during controller design.

$$\begin{aligned} w_e &= \frac{s^2/M_s+2\xi w_b s/\sqrt{M_s}+w_b^2}{s^2+2\xi w_b s\sqrt{\varepsilon}+w_b^2\varepsilon}, \\ M_s &= 3.162,\ \varepsilon = 0.01,\ \xi = 0.5, w_b = 2\pi \times 10 \end{aligned} \tag{14}$$

$$w_u = \frac{s + w_{bc}/M_u}{\varepsilon_1 s + w_{bc}}, M_u = 100, \varepsilon_1 = 0.01, w_{bc} = 2\pi \times 1200 \tag{15}$$

$$W_e = \begin{bmatrix} w_e & 0 \\ 0 & w_e \end{bmatrix},\ W_u = \begin{bmatrix} w_u & 0 \\ 0 & w_u \end{bmatrix} \tag{16}$$

5.2. Uncertainty weight selection

In this paper, output multiplicative uncertainty is used for model set representation [14]. Firstly, the frequency responses of the azimuth and elevation axes are obtained by using swept sine tests. These tests are carried out at different excitation levels and around different gimbal positions. In this way, different linearized models corresponding to different operating conditions are obtained. Magnitude and phase responses of the two axes corresponding to five different tests can be found in Figure 7. Next, using these responses and nominal models, five different multiplicative perturbations are found. After that, stable transfer functions (17) and (18) that upper bound these perturbations are obtained. These perturbations and upper bounds are displayed in Figure 8. While evaluating the robustness of the stabilization loop, the transfer matrix

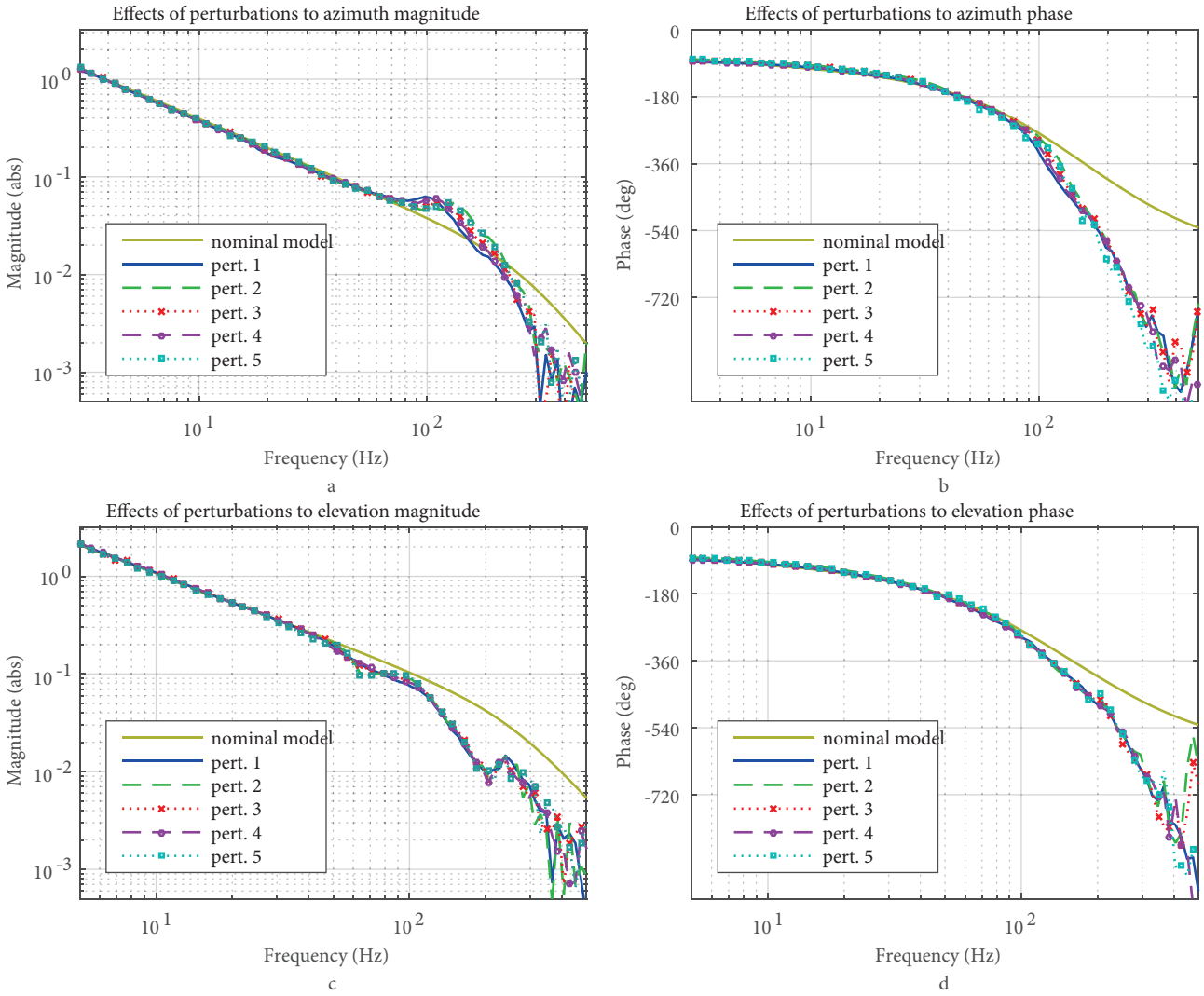

Figure 7. Effect of perturbations to (a) azimuth magnitude, (b) azimuth phase, (c) elevation magnitude, (d) elevation phase.

(19) is used [13].

$$w_{1a} = \frac{1.87s^2 + 792.65s + 90750}{1s^2 + 650.35s + 572624} \tag{17}$$

$$w_{1e} = \frac{1.12s^2 + 2564.28s + 289957}{1s^2 + 2059.65s + 2375266} \tag{18}$$

$$W_1 = \begin{bmatrix} w_{1a} & 0 \\ 0 & w_{1e} \end{bmatrix} \tag{19}$$

Figure 8 and (17) and (18) suggest that at low frequencies the uncertainties are around 0.15 and 0.12 for azimuth and elevation models, respectively. Due to structural resonances, the uncertainties exceed 1 around 100 Hz and 200 Hz for azimuth and elevation. These results are very similar to the observations reported in [17].

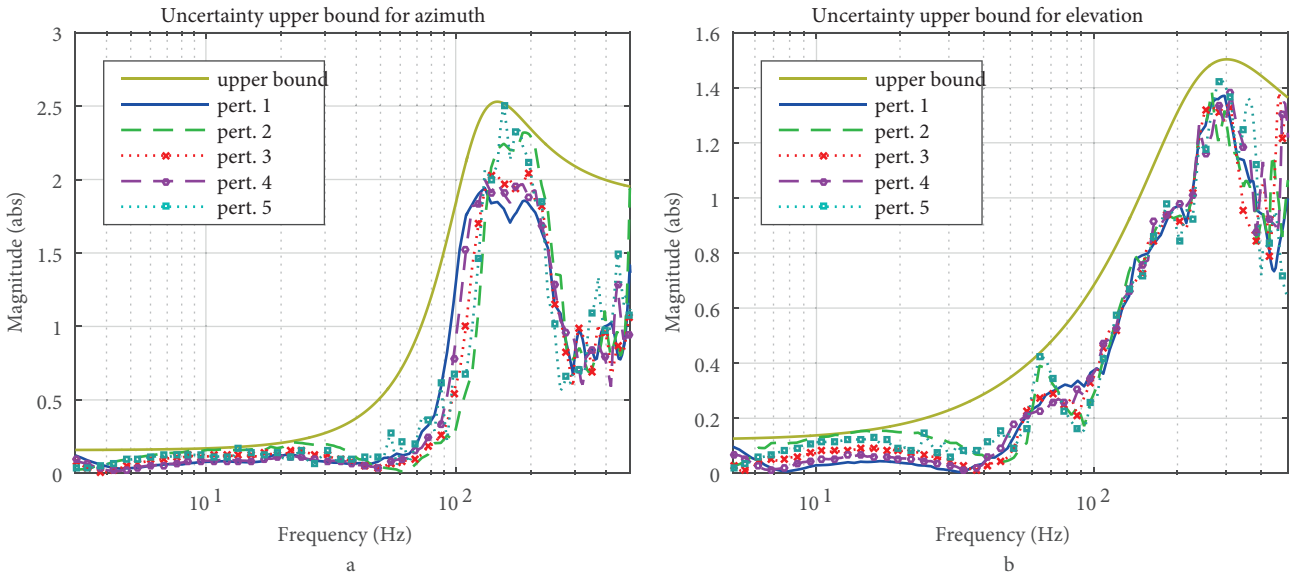

Figure 8. Uncertainty upper bounds for (a) azimuth, (b) elevation.

6. Comparison of controller

In section 2, three different controller design methods were reviewed. Each method uses transfer matrices to weight different signals. Table 2 summarizes all these matrices for three methods. Using these weights, LQG/LTR, H_∞, and μ controllers are designed. Next, robustness of the designs is investigated in this section.

Table 2. Selected weights.

LQG/LTR design: $D^{1/2} = W_e$, $V^{1/2} = I$
H_∞ design: $W_e = W_e$, $W_u = W_u$, $W_t = W_1$
μ-Synthesis design: $W_e = W_e$, $W_u = W_u$, $W_p = W_1$

The robustness analysis is usually performed by investigating the structured singular value (μ) of the closed loop system (μ-analysis). In this section, the LFT structure given in Figure 3 is used, where the performance criterion is the H_∞ norm inequality (20).

$$\left\| \begin{bmatrix} W_e S_o \\ W_u K S_o \end{bmatrix} \right\|_\infty < 1 \tag{20}$$

To conduct a robust performance test, a fictitious perturbation block is introduced to connect error signal e and exogenous signal w. Therefore, a modified uncertainty block (21) is constructed to analyze robust performance. After that, the lower LFT of Figure 3 is found. The MΔ structure is constructed with matrices (21) and (22) and it is used for μ-analysis [14,15].

$$\tilde{\mathbf{\Delta}} = \left\{ diag\left[\mathbf{\Delta}\,,\, \mathbf{\Delta}_p\right] : \mathbf{\Delta} \in \mathrm{C}^{2\,x\,2}, \mathbf{\Delta}_p \in \mathrm{C}^{2\,x\,4} \right\} \tag{21}$$

$$M = \begin{bmatrix} M_{11} & M_{12} \\ M_{21} & M_{22} \end{bmatrix},\ M_{11}, M_{12} \in \mathrm{C}^{2\,x\,2},\ \ M_{21}, M_{22} \in \mathrm{C}^{4\,x\,2} \tag{22}$$

$$NP \Leftrightarrow \bar{\sigma}\left(M_{22}\right) = \mu_{\mathbf{\Delta}_p} < 1, \forall w \tag{23}$$

$$RS \Leftrightarrow \mu_{\mathbf{\Delta}}\left(M_{11}\right) < 1, \forall w \tag{24}$$

$$RP \Leftrightarrow \mu_{\tilde{\mathbf{\Delta}}}\left(M\right) < 1, \forall w \tag{25}$$

Inequalities (23) to (25) are the nominal performance (NP), robust stability (RS), and robust performance (RP) μ tests for a nominally stable system, respectively [15,18]. Now, using these tests, the robustness of the three designs is investigated. First, the nominal performances, robust stabilities, and robust performances are depicted in Figure 9a and 9b. Next, to compare the controllers, their singular values are illustrated in Figure 9c.

Figure 9 suggests the following:

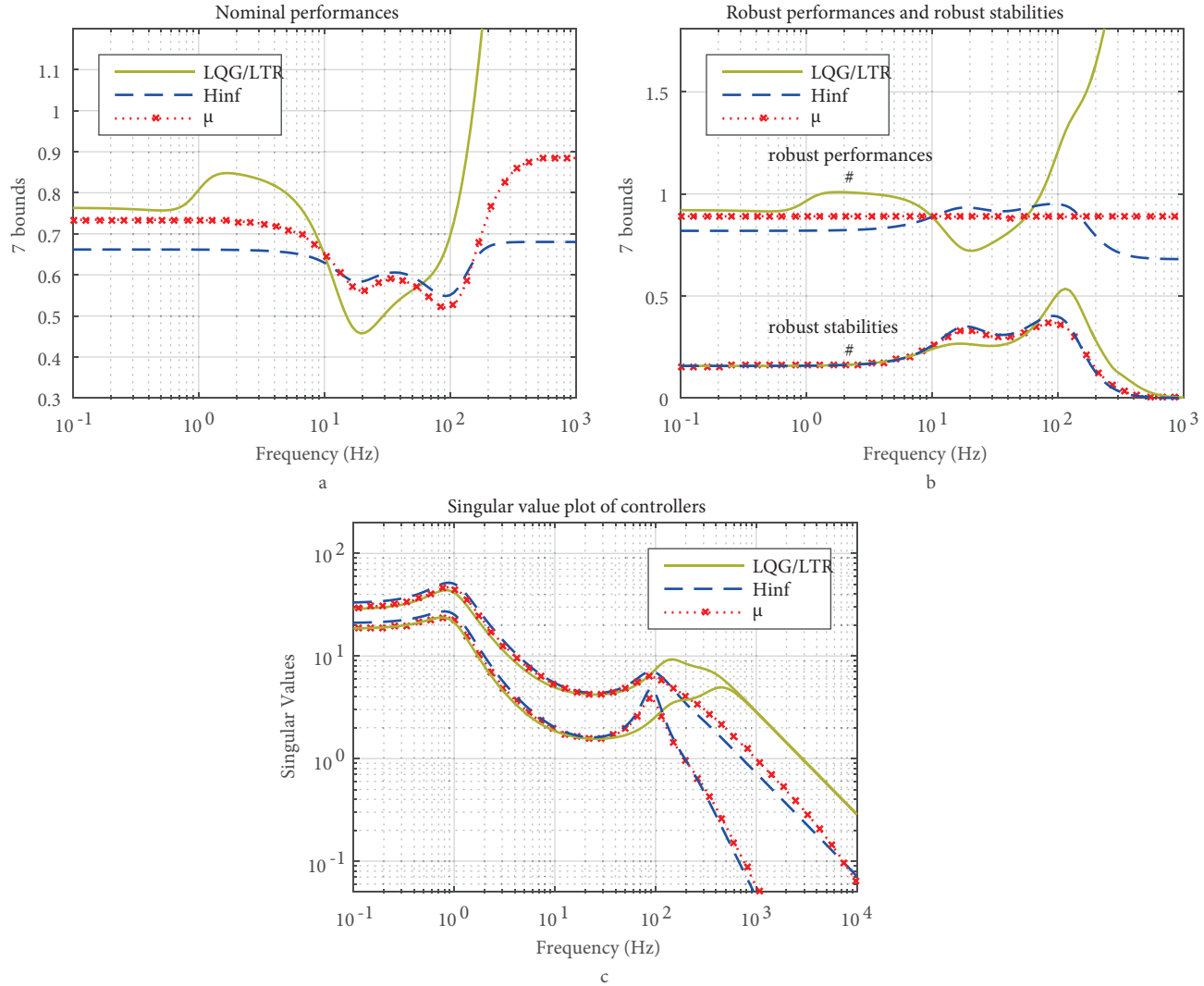

Figure 9. Comparison of different controllers (a) nominal performances, (b) robust performances and robust stabilities, (c) controllers.

The LQG/LTR controller satisfies the robust performance condition in low frequencies where the weighted sensitivity ($W_e S_o$) dominates the cost function (7). However, at high frequencies the performance decreases significantly since there is no KS_o dependent term in the LTR cost function (5). In this aspect, the LQG/LTR controller gives good results if the performance index includes weighted sensitivity alone [3].

The H_∞ controller satisfies the robust stability and performance condition, and its performance is the highest in both low and high frequency regions. However, around the crossover region, the μ controller outperforms the H_∞ controller.

As shown in Figures 2 and 3, H_∞ and μ-synthesis designs use the same structure when complementary sensitivity weight is equal to perturbation upper bound. Therefore, the H_∞ controller is simply the μ controller at the first $D-K$ iteration. In this aspect, it can be concluded that the D-K iterations minimize the peak of the robust performance. That is, μ values are flattened after a new iteration. However, this method achieves that by reducing nominal performance.

7. Implementation of controllers

Each design method produces a controller whose order is equal to generalized plant order [15]. For that reason, a 14th order LQG/LTR controller, 20th order H_∞ controller, and 32nd order μ controller are designed [13]. The implementations of these high order controllers are difficult tasks. Furthermore, they lead to high process cost and poor reliability in the system. In this aspect, lower order controllers are obtained without allowing significant performance change. Balance model truncation is applied, and 12th order controllers whose transfer matrices are given in the appendix are obtained for each design. After that, these reduced order controllers are discretized by Bilinear transform, and they are programmed into a digital computer.

8. Experimental results

The actual performances of the designed controllers are investigated on the test setup in Figure 5. During tests, fictitious disturbance is applied at the plant output by signal analyzer and corresponding angular speed responses are measured.

The output equation of the classical closed loop system is given in (26). If reference r, noise n, and input disturbance d_i are neglected, a simple equation (27) is obtained for a two-axis gimbal.

$$y = T_o\,(r-n) + S_o P d_i + S_o d \tag{26}$$

$$\begin{bmatrix} w_{az} \\ w_{el} \end{bmatrix} = \begin{bmatrix} So_{11} & So_{12} \\ So_{21} & So_{22} \end{bmatrix} \begin{bmatrix} d_{az} \\ d_{el} \end{bmatrix} \tag{27}$$

Using the implemented controllers, a closed loop system is constructed each time. Next, closed loop sensitivity responses are obtained by using swept sine tests with different disturbance levels and around different gimbal positions. For example, when the elevation disturbance d_{el} is zero, sinusoidal disturbance signal d_{az} is applied to the azimuth channel. Although the control loops minimize this disturbance, LOS moves with angular speeds w_{az} and w_{el}. In this way, by applying disturbance at different frequencies, responses of S_{o11} and S_{o21} are determined. Similarly, when d_{az} is zero and d_{el} is applied, responses of S_{o12} and S_{o22} are found. After that, the frequency response of S_o is obtained by constructing matrices at a grid of frequencies. Next, the performance (28) is evaluated for each case. As discussed previously, performance is satisfied if (28) must be smaller than 1. The experimental results are illustrated in Figure 10 for three designs.

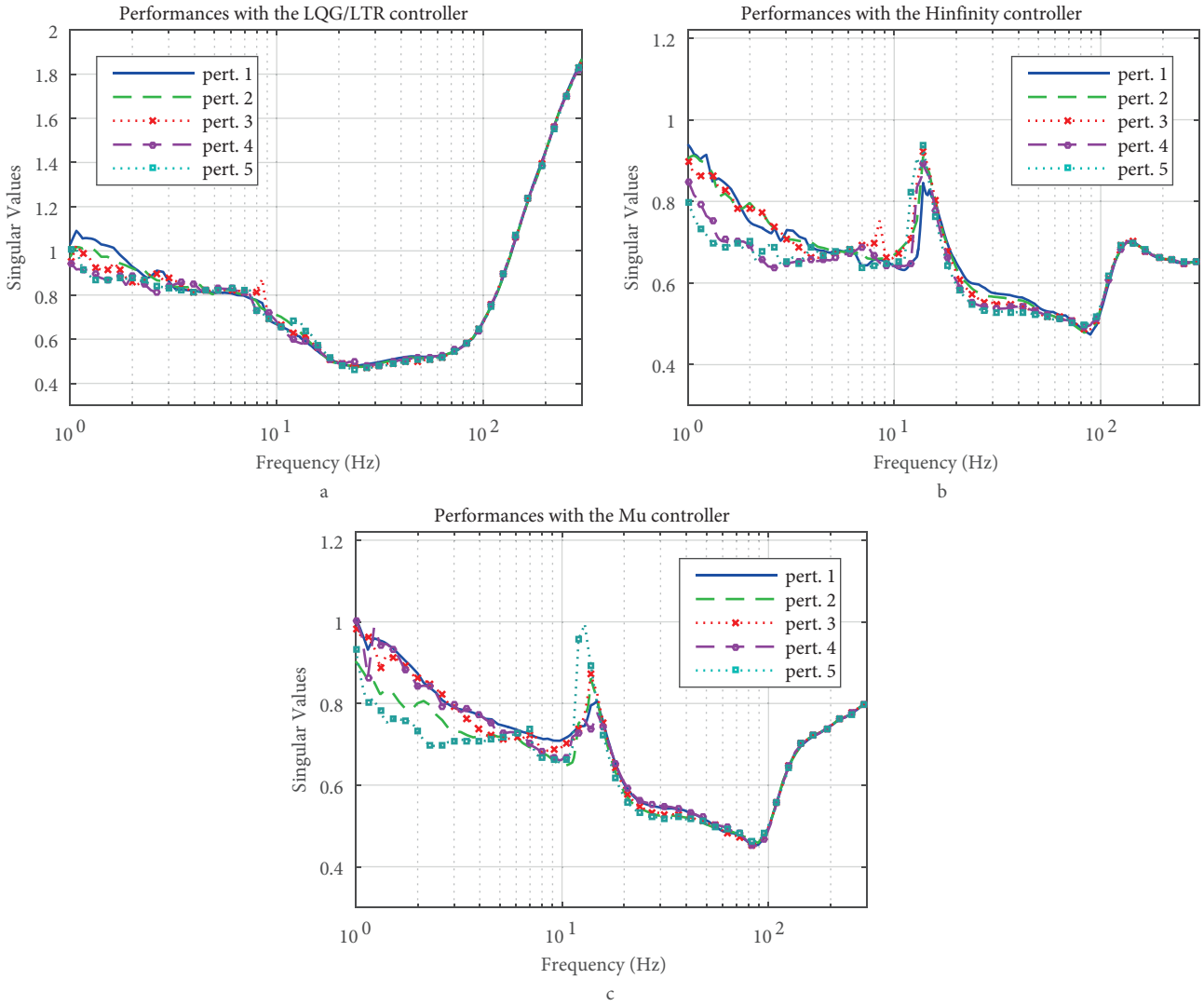

Figure 10. Performances of perturbations with (a) LQG/LTR controller, (b) H_∞ controller, (c) μ controller.

$$\left\| \begin{bmatrix} W_e S_o \\ W_u K S_o \end{bmatrix} \right\|_\infty \tag{28}$$

The theoretical performances were given in Figure 9 before. The experimental results show similar characteristics. At low frequencies, the best performance is obtained from the H_∞ controller due to highest controller gain in this region. Moreover, at high frequencies the performance of the LQG/LTR controller degrades due to high controller gains. Apart from that, around crossover the μ controller is better than the H_∞ controller, and at high frequencies the H_∞ controller is the best one due to the highest roll off rate.

When the experimental findings are investigated, it is seen that performance degrades around 15 Hz due to small azimuth resonance. This shows that around this resonance uncertainty in the model is larger than the one authors found in Section 5.

Please note that robust performance is satisfied if the performance condition (20) is satisfied for all model

perturbations. Since all performances corresponding to different perturbations are smaller than 1 in Figure 10, it is accepted that the H_∞ and μ controllers satisfy robust performance. Moreover, similar to theoretical results the LQG/LTR controller could not satisfy the performance requirement at high frequencies.

9. Conclusion

By looking at the theoretical and experimental results, it can be said that the designed controllers satisfy the performance and stability requirements. One may observe that each control method discussed in this paper tries to minimize some cost function. The LQG/LTR method minimizes the total of nominal performance and robust stability over all frequencies. On the other hand, the H_∞ design minimizes the worst case nominal performance and robust stability. Finally, μ-synthesis attempts to minimize the worst case robust performance. However, there are trade-offs in feedback systems. In other words, it is not possible to obtain good performance in all these aspects at the same time. For example, a small robust performance peak comes with reduced nominal performance. In a similar way, reducing nominal performance may lead to poor robust stability and robust performance. In this aspect, the following conclusions can be reached:

When the robustness at low frequencies is important one can use the H_∞ controller. If the robust performance over all frequencies is essential, the μ controller should be chosen. One can prefer the H_∞ controller over the μ controller if the worst case perturbation is unlikely to occur. In converse conditions, μ controller selection is reasonable. When performance is measured by weighted sensitivity alone, the LQG/LTR controller can be used because of its simplicity and it gives results similar to the H_∞ controller [3]. However, if the performance index is more complicated, the LQG/LTR controller should be the third choice due to its poorest stability and performance properties at high frequencies.

Acknowledgment

The support and facilities provided by ASELSAN Inc. are gracefully appreciated.

References

[1] Kennedy P, Kennedy R. Line of Sight Stabilization Primer. Peter Kennedy, 2012.

[2] Masten M. Inertially stabilized platforms for optical imaging systems. IEEE Contr Syst Mag 2008; 28: 47-64.

[3] Baskın M, Leblebicioğlu K. Robust stabilization loop design for gimbaled electro-optical imaging system. arXiv preprint arXiv:1602.06832, 2016.

[4] Seong K, Kang H, Yeo B, Lee H. Q, Xia Y, Liu X. The stabilization loop design for a two-axis gimbal system using LQG/LTR controller. In: SICE-ICASE International Joint Conference, 2006.

[5] Xiao R, Li Tao, Zhang P, Jia X, Qin Y, Xian C. The LQG/LTR controller design for miniaturized infrared stabilizing platform. In: International Symposium on Photoelectronic Detection and Imaging 2011: Advances in Infrared Imaging and Applications, 2011.

[6] Moorty K, Marathe R, Sule V. H∞ control law for line-of-sight stabilization for mobile land vehicles. Opt Eng 2002; 41: 2935-2944.

[7] Liu Z, Bao Q, Xia Y, Liu X. H∞ mix sensitivity controller design based on GIMC for electro-optical stabilization and tracking system. In: International Symposium on Photoelectronic Detection and Imaging 2013: Laser Communication Technologies and Systems, 2013.

[8] Kim S, Kim S, Kwak Y. Robust control for a two-axis gimbaled sensor system with multivariable feedback systems. IET Control Theory A 2010; 4: 539-551.

[9] Bao W, Huang X, Ban X. Control system design of multi-gimbal electro-optical platform by the technique of μ-synthesis. In: IEEE 29th Chinese Control Conference; 2010; pp. 3447-3452.

[10] Maciejowski J. Multivariable Feedback Design. Wokingham, UK: Addison-Wesley, 1989.

[11] Stein G, Athans M. The LQG/LTR procedure for multivariable feedback control design. IEEE T Automat Contr 1987; 32: 105-114.

[12] Doyle J, Stein G. Multivariable feedback design: concepts for a classical/modern synthesis. IEEE T Automat Contr 1981; 26: 4-16.

[13] Baskın M. LQG/LTR, H-infinity and Mu robust controllers design for line of sight stabilization. MSc, Middle East Technical University, Ankara, Turkey, 2015.

[14] Zhou K, Doyle J. Essentials of Robust Control. Upper Saddle River, NJ, USA: Prentice Hall, 1998.

[15] Skogestad S, Postlethwaite I. Multivariable Feedback Control. Chichester, UK: Wiley, 2005.

[16] Ekstrand B. Equations of motion for a two-axes gimbal system. IEEE T Aero Elec Sys 2001; 37: 1083-1091.

[17] Özdoğan G, Leblebicioğlu K. Frequency response function measurement and parametric SISO system modelling of a gyro-stabilized infrared electro optic gimbal system. T I Meas Control 2016; 38: 512-528.

[18] Packard A, Doyle J. The complex structured singular value. Automatica 1993; 29: 71-109.

Appendix

The designed controllers can be represented with a transfer matrix as given in (A.1), where the transfer functions K_{12} and K_{21} are approximately zero due to the decoupled azimuth and elevation axes. ($K_{12}(s) \approx 0$ and $K_{21}(s) \approx 0$). Therefore, only the transfer functions $K_{11}(s)$ and $K_{22}(s)$ are given in zero-pole-gain form below.

$$K(s) = \begin{bmatrix} K_{11}(s) & K_{12}(s) \\ K_{21}(s) & K_{22}(s) \end{bmatrix} \tag{A.1}$$

LQG/LTR controller:

$$K_{11}(s) = \frac{18058(s+580.7)(s+49.67)(s+5.364)(s^2+1315s+1.1e06)}{(s^2+5.974s+35.42)(s^2+686.3s+7.599e05)(s^2+2828s+4.017e06)}$$

$$K_{22}(s) = \frac{17685(s+429.1)(s+54.56)(s+8.837)(s^2+1099s+1.659e06)}{(s^2+5.941s+34.97)(s^2+869.9s+1.226e06)(s^2+3560s+7.695e06)}$$

H_∞ controller:

$$K_{11}(s) = \frac{4538.3(s+63.75)(s+19.62)(s+5.569)(s^2+822.9s+2.679e05)}{(s+946.9)(s+20.2)(s^2+6.25s+39.7)(s^2+482.3s+3.386e05)}$$

$$K_{22}(s) = \frac{8.7794(s+1.949e05)(s+65.15)(s+9.314)(s^2+1256s+5.537e05)}{(s^2+6.284s+39.5)(s^2+221.8s+3.361e05)(s^2+2059s+2.068e06)}$$

μ controller:

$$K_{11}(s) = \frac{1078.7(s+2.26e05)(s+54.11)(s+5.454)(s^2+527.1s+1.779e05)}{(s+3.746e04)(s+1169)(s^2+6.281s+39.56)(s^2+454.7s+2.492e05)}$$

$$K_{22}(s) = \frac{0.094293(s+2.408e07)(s+58.72)(s+9.12)(s^2+1178s+5.234e05)}{(s^2+6.279s+39.25)(s^2+267.9s+3.354e05)(s^2+2558s+2.623e06)}$$